Observation of Bose–Einstein condensates in an Earth-orbiting research lab

https://doi.org/10.1038/s41586-020-2346-1
Received: 30 October 2019
Accepted: 26 March 2020

Published online: 11 June 2020
Check for updates

David C. Aveline[1,2]✉, Jason R. Williams[1,2], Ethan R. Elliott[1,2], Chelsea Dutenhoffer[1], James R. Kellogg[1], James M. Kohel[1], Norman E. Lay[1], Kamal Oudrhiri[1], Robert F. Shotwell[1], Nan Yu[1] & Robert J. Thompson[1]✉

Quantum mechanics governs the microscopic world, where low mass and momentum reveal a natural wave–particle duality. Magnifying quantum behaviour to macroscopic scales is a major strength of the technique of cooling and trapping atomic gases, in which low momentum is engineered through extremely low temperatures. Advances in this field have achieved such precise control over atomic systems that gravity, often negligible when considering individual atoms, has emerged as a substantial obstacle. In particular, although weaker trapping fields would allow access to lower temperatures[1,2], gravity empties atom traps that are too weak. Additionally, inertial sensors based on cold atoms could reach better sensitivities if the free-fall time of the atoms after release from the trap could be made longer[3]. Planetary orbit, specifically the condition of perpetual free-fall, offers to lift cold-atom studies beyond such terrestrial limitations. Here we report production of rubidium Bose–Einstein condensates (BECs) in an Earth-orbiting research laboratory, the Cold Atom Lab. We observe subnanokelvin BECs in weak trapping potentials with free-expansion times extending beyond one second, providing an initial demonstration of the advantages offered by a microgravity environment for cold-atom experiments and verifying the successful operation of this facility. With routine BEC production, continuing operations will support long-term investigations of trap topologies unique to microgravity[4,5], atom-laser sources[6], few-body physics[7,8] and pathfinding techniques for atom-wave interferometry[9–12].

With the launch and operation of the Cold Atom Lab (CAL), NASA has established the sustained study and development of quantum technologies in orbit. This versatile, multi-user research facility has travelled over 400 million kilometres on board the International Space Station (ISS) since June 2018, under remote operation from the Jet Propulsion Laboratory. Exploiting the microgravity environment of space, researchers can utilize the full sensitivity of ultracold matter-waves to explore fundamental physics and the organizing principles of complex systems from which structure and dynamics emerge—executing major 'thrusts' of the National Research Council's Decadal Survey that define the frontier of space-based fundamental physical science[13].

Understanding quantum mechanics has made possible the now-ubiquitous technologies of lasers, semiconductors and transistors, but remaining elusive is its relationship with general relativity, the physics of gravity, which is well understood at macroscale to astronomic scales. Scaling quantum mechanics to macroscopic sizes is a primary goal of cooling atomic gases towards absolute zero, where wave-like behaviour markedly increases as temperature drops. With enough cooling, each atom's wavelength approaches the interparticle spacing and the system exhibits the macroscopic quantum behaviour of superfluidity. For a dilute gas of bosons—the type of atoms contained in CAL—this phenomenon is known as Bose–Einstein condensation. These quantum gases, and particularly BECs, have been studied for their intrinsic properties, used as analogues of more inaccessible systems, or applied as inertial sensing matter waves. The state-of-the-art technology has advanced to such a degree that additional cooling techniques are stifled by gravity. For example, the confining potentials that trap the atoms can be adiabatically decompressed to decrease temperature, but only until the local potential minimum is collapsed by gravity's asymmetric pull. Furthermore, following release from an atom trap, gravity-induced centre-of-mass motion greatly limits the system's utility as an inertial sensor. The ideal conditions for engineering macroscopic atom-waves thus becomes ultracold temperatures combined with reduced gravity.

Pioneering cold-atom experiments have mitigated the effects of gravity through a variety of methods. Ground-based levitation techniques accomplish a localized counter-balance to gravity in decompression experiments[1], but they introduce mass- and state-dependent forces that broadly limit atom-wave interferometry and tests between multiple atomic species. Because cold-atom experiments require an ultrahigh vacuum (UHV) to thermally isolate the atoms from the ambient environment, the primary solutions are either to enlarge the size of the UHV chamber or increase the free-fall time of the entire apparatus. Ground-based interferometers have achieved state-of-the-art

---

[1]Jet Propulsion Laboratory, California Institute of Technology, Pasadena, CA, USA. [2]These authors contributed equally: David C. Aveline, Jason R. Williams, Ethan R. Elliott.
✉e-mail: David.C.Aveline@jpl.nasa.gov; Robert.J.Thompson@jpl.nasa.gov

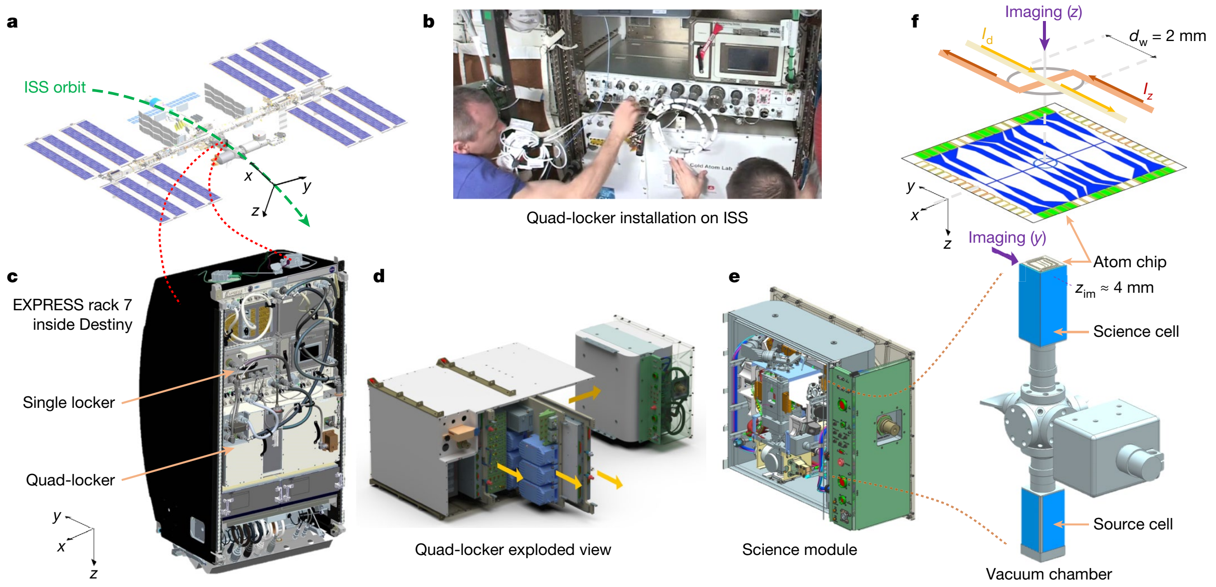

Fig. 1 | CAL hardware configuration. **a**, The CAL payload resides in an 'EXpedite the PRocessing of Experiments to the Space Station' (EXPRESS) rack within the US Lab Destiny Module, located where shown in the ISS. The *x*, *y*, *z* coordinates are illustrated. **b**, The payload was installed by astronauts during a 6-h crew operation under guidance from JPL (image source: NASA). **c**, View of EXPRESS rack 7. CAL is packaged within this rack in a single locker and a quad-locker, requiring one and four payload slots, respectively. The single locker houses the power electronics, while the quad-locker contains the computer, laser sources, optical control network, control electronics and the magnetically shielded science module. **d**, An exploded view of the quad-locker, illustrating its modular design, including drawer access to lasers and electronics from the front, and the science module to the right. **e**, An inside view of the science module, without the front half-shell of the magnetic shields. **f**, At the heart of the science module, an aluminium optical bench holds a dual-cell vacuum chamber. Forming the top wall of the UHV science cell is an atom chip, which can generate re-configurable magnetic traps with its current-carrying wires. The primary trap is centrally located on a window of diameter $d_w = 2$ mm, formed by chip currents I_z and I_d. This optical access allows absorption imaging along the *z* axis, while CAL's primary imaging is accomplished along the *y* axis centred at $z_{im} \approx 4$ mm below the chip (purple arrows). See Methods and Extended Data Fig. 1 for more details about the optical beams.

interrogation times and temperatures by launching atoms in a stationary 10-m-tall UHV chamber[14,15]. In contrast, portable cold-atom systems that are compact and ruggedized have realized temporary free-fall through drop towers[16–18], Einstein elevators[19], zero-*g* aircraft[20,21] and suborbital launch vehicles[22–26]. Notably, six minutes of microgravity achieved in a sounding rocket in parabolic flight above the Kármán line (the altitude of 100 km above sea level, which is considered the boundary of space) demonstrated production and manipulation of BECs[26]. For these portable instruments to advance in scope and capability, their operation times and repetition rates must increase. As the natural next step, new generations of quantum experiments seek to operate a versatile ultracold atomic physics lab in the persistent microgravity conditions of low Earth orbit[3]. Space missions enable large variations of velocity and gravitational potential compared to ground-based laboratories, inspiring many proposed missions. These concepts include tests of Einstein's equivalence principle with quantum proof masses[27,28], gravitational wave detection that could complement the Laser Interferometer Space Antenna (LISA)[29–32], optical atomic clocks for a 'world-clock'[33], direct detection of dark matter and dark energy candidates[27,34], geodesy, Earth and planetary sciences[35–37] and advanced navigation capabilities[37–39].

The realization of an off-world cold-atom instrument presents new technical challenges. It not only calls for robust hardware adhering to the stringent size, weight and power requirements of a spaceborne instrument, but must also reliably and autonomously operate for years without manual intervention. In addition to technological maturation (unique aspects and challenges in developing this Earth-orbiting cold-atom facility are elaborated in Methods), long-term operation allows adjustment and adaptation of the precise procedures and protocols needed to control atoms in microgravity. The capabilities of the CAL instruments enable multiple teams of scientists to study quantum gases at unprecedented low energies and densities produced in weakly confining traps. The ^{87}Rb BECs we report here will specifically support investigations of atom laser sources[6,9], bubble-shell topologies unique to microgravity[4,5] and advanced techniques for Earth-orbiting atom interferometry including delta kick cooling[9] and novel decompression protocols[10,11].

Following its launch on 21 May 2018 on the OA-9 Antares 230 rocket, the CAL hardware was installed and fully powered on board the ISS by June 2018, commencing daily operation as the first ultracold atom system in orbit. As described in ref. [40], the instrument is composed of three primary subsystems: the science module, the laser and optics system, and the electronics, supported by thermal, mechanical and software control, all designed for modular integration into a standardized ISS equipment rack (see Fig. 1). Re-configurable traps that hold and manipulate cold atoms are created by the current-carrying wires of an 'atom chip' that forms the top wall of a rectangular glass cell under UHV[41]. Wire-loop emitters positioned near the ambient surface of the chip transmit radio frequency (RF) or microwave radiation for evaporative cooling and state preparation. Further instrument details can be found in Methods and Extended Data Fig. 1.

Implementing the same stages of laser cooling and magnetic trapping of ^{87}Rb in the state $|F=2, m_F=2\rangle$, as executed on the ground[40], we find that RF-induced evaporative cooling (see Methods) reveals markedly different results in microgravity. Figure 2 shows a terrestrial BEC produced before the launch of CAL compared to an evaporated atom cloud on the ISS. We observe an on-orbit increase in the atom number of nearly threefold. Through the application of varied magnetic field gradients, we confirm that approximately half of the atoms are in the magnetically insensitive state $|2, 0\rangle$, forming a halo-like cloud around the location of the magnetic trap. On Earth, the dominating force acting on atoms in this $|2, 0\rangle$ state is gravity. In microgravity, however, the dominant force acting on these $|2, 0\rangle$ atoms is due to the quadratic Zeeman (QZ) effect, given by[42] $h\cdot(287.58\ \text{Hz G}^{-2})\cdot B^2$.

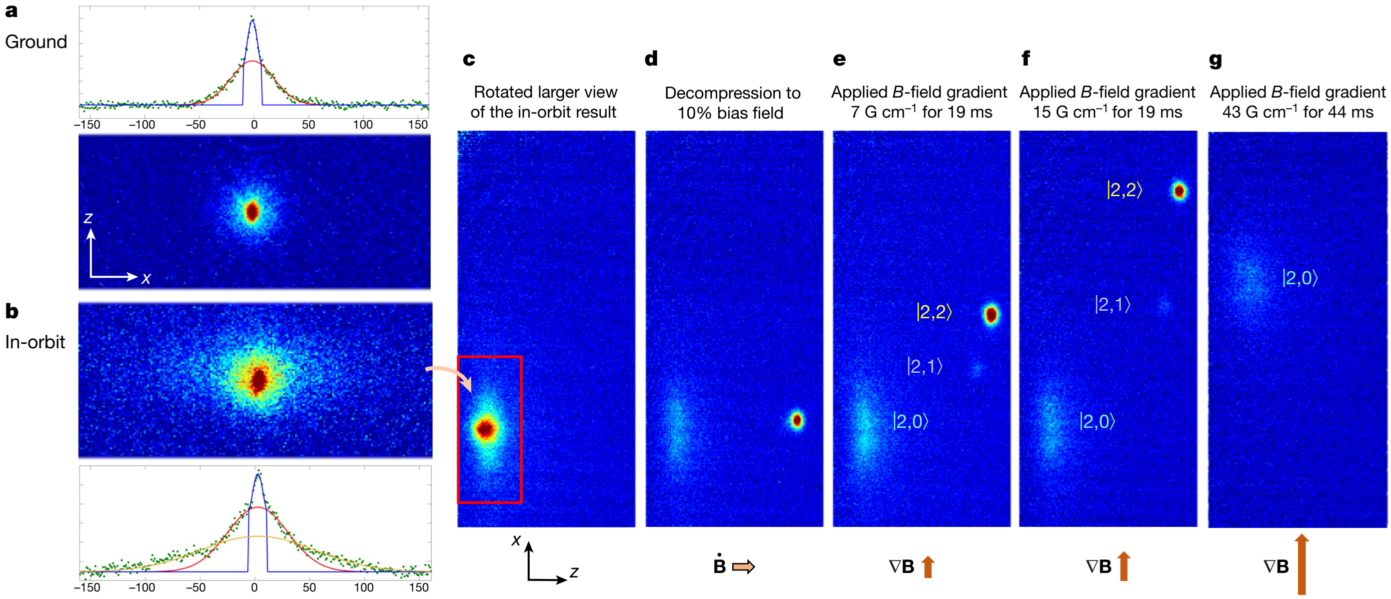

Fig. 2 | BEC production in CAL on the Earth and in orbit. a, A false-colour absorption image shows a BEC produced in CAL on the ground at 22 ms TOF, totalling 4.5×10^4 atoms and a BEC fraction of 15%. **b**, Likewise, a BEC at 22 ms TOF produced in CAL on board the ISS using the same parameters as on the ground, totalling 1.3×10^5 atoms, shows that a large portion of these atoms have a density profile distinctly different from the expected bimodal distribution. Plots adjacent to the images **a** and **b** show the data (green) of column density along pixels of the x axis. Fits indicate the condensate (blue), thermal cloud (red), and residual halo-cloud (orange) of |2, 0⟩ atoms. **c**, A larger region of interest than shown in **b**, using the same production sequences except for changes to the release procedure as follows (**d**–**g**). **d**, Released atoms with the location of the trap bottom moved 0.65 mm away from the surface of the chip. A magnetically insensitive halo-cloud of |2, 0⟩ atoms is left behind during this re-positioning of the primary trap bottom. **e**, **f**, The same decompression procedure as shown in **d**, but followed by applying a transverse gradient of 7 G cm^{-1} (**e**) or of 15 G cm^{-1} (**f**) for the first 19 ms of a 22-ms TOF. The halo-cloud remains unmoved. A faint cloud of |2, 1⟩ atoms that was weakly confined in the trap experiences less acceleration and trails halfway behind the |2, 2⟩ atoms. **g**, The same decompression procedure as shown in **d**, but followed by application of a stronger transverse gradient of 43 G cm^{-1} for the first 44 ms of a 50-ms TOF, which accelerates the |2, 0⟩ cloud due to the QZ effect[42]. An arrow below each panel **d**–**g** illustrates the directional force applied by incremental changes in magnetic fields, dynamically, $\dot{\mathbf{B}}$, or spatially, $\nabla\mathbf{B}$.

Increasing the applied field gradient to approximately $\nabla B = 43$ G cm^{-1}, we demonstrate motion of the |2, 0⟩ halo-cloud due to this QZ effect (Fig. 2g). Further incidental QZ forces acting on the |2, 0⟩ halo-cloud throughout the standard operation of our chip-based trap (owing to its large magnetic fields and gradients) are discussed below. By controlled manipulation and isolation of the atoms in the |2, 0⟩ state, we readily confirm production of ^{87}Rb |2, 2⟩ BECs in orbit. Figure 3 illustrates the onset of condensation as cloud temperature is reduced below the BEC transition temperature. Tell-tale signatures of condensation include the sudden onset of a bimodal density distribution below the theoretically predicted critical temperature at long time of flight (TOF), and a dense elliptical core (anisotropic expansion) surrounded by a thermal gas background (isotropic expansion).

Taking advantage of the intrinsic advantages of microgravity, we demonstrate a combination of low temperatures and extended free-space expansion times with only minor readjustments to our pre-launch procedures. Beginning from a nominal ^{87}Rb BEC, we decompress the trap, transfer the atoms to a magnetically insensitive state, and release the atoms with parameters empirically adjusted in orbit to minimize the temperature and drift velocity of the atom cloud in free-fall. We benefit from the relatively high repetition rate (once per minute) and extended experimental time available on the ISS to make these adjustments, receive real-time feedback, and modify accordingly. Decompression is carried out by two stages of linear reduction to the bias fields applied by the external coils, thereby decreasing the trap frequency and translating the trap centre approximately 1 mm away from the chip (see Methods).

Images of atoms, along with the respective cloud positions and widths, during free expansion up to 1.118 s are shown in Fig. 4, with the residual expansion of the BEC corresponding to a kinetic energy temperature equivalent of 231(9) pK (720(79) pK) in the direction parallel (normal) to the chip surface. In the earliest expansion time shown in Fig. 4a, the halo-cloud of |2, 0⟩ produced during evaporation is also present, coasting away from the chip with the motion imparted by the QZ effect when the location of the trap bottom shifts during decompression. Producing this combination of low temperatures and long expansion times using a simple adjustment to our ground procedure demonstrates not only the natural benefit of microgravity, but also the ability to rely on empirically derived optimization over the course of days, as well as the potential for further improvements. As CAL science operations continue, investigators will take further advantage of microgravity by introducing more complex decompression curves, allowing greater adiabaticity, less residual centre-of-mass motion, lower temperatures and subhertz trapping frequencies.

The next generation of ultracold gas experiments using weak traps may also benefit from further studies of the observed halo-cloud of |2, 0⟩ atoms. We note that the halo-cloud is shaped by a combination of factors: the initial temperature and density distribution of the trapped atoms, the momentum distribution of |2, 0⟩ as they are generated by in situ RF coupling, and finally the dominating forces due to the QZ effect in the presence of the chip's strong magnetic fields and gradients. An atom that undergoes a forced-evaporation transition into the |2, 0⟩ state by application of resonant RF radiation ('RF knife') would lose potential energy equal to the magnetic trap depth and propagate with kinetic energy proportional to k_BT plus a new, lower potential energy determined by the QZ effect. In the present work, the magnetic fields during evaporation form an attractive QZ potential for atoms in the |2, 0⟩ state with 18 μK depth and aspect ratio ≤0.2 (see Methods). The timescales on which we currently observe the halo-clouds are consistent with confinement and subsequent release from such a trap in

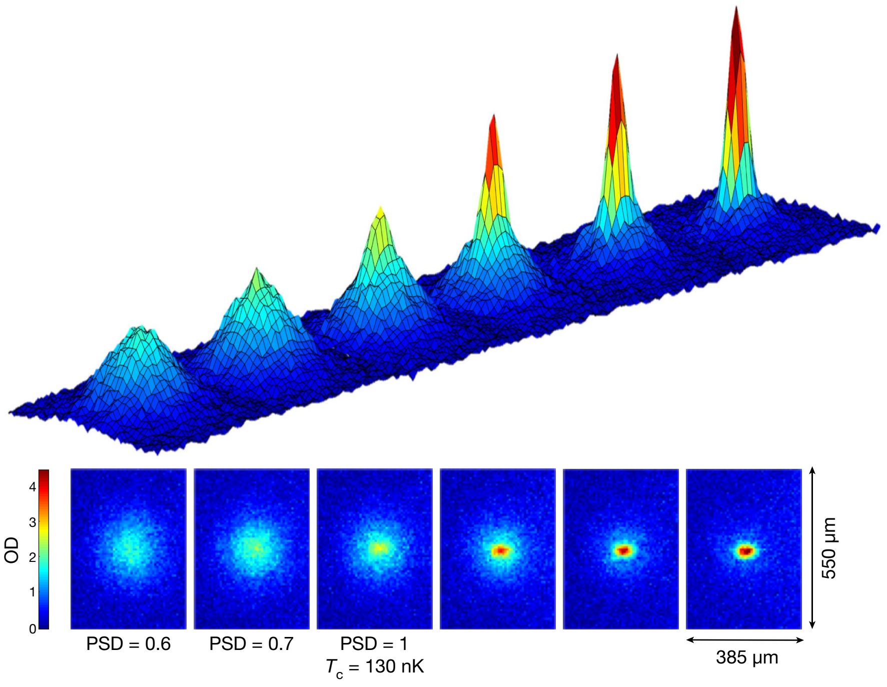

Fig. 3 | Onset of Bose–Einstein condensation in low Earth orbit. False-colour absorption images of ^{87}Rb atomic clouds evaporated and released from CAL's magnetic atom chip trap are displayed as surface plots (top) and corresponding arrays (bottom). OD indicates optical density. From left to right, the final frequency of a forced evaporation ramp using an RF knife in a magnetic atom chip trap is lowered, increasing the phase space density (PSD) and forming a BEC marked by a signature spike in the central density. At the conclusion of the evaporation ramp, the magnetic trap potential is decompressed and extinguished before imaging the atoms 22 ms later. The BEC critical temperature (T_c) is 130 nK (corresponding to 500 nK in the original trap). The rightmost image shows an atom cloud with 4.9×10^4 total atoms, 26% condensed in a BEC at a temperature of 17 nK measured from the distribution of the surrounding thermal cloud.

microgravity, which is normally overpowered by gravitational sag in our measurements on Earth. We note that a low-frequency anharmonic trap naturally formed and populated with large numbers of magnetically insensitive atoms throughout the evaporation process is an intriguing alternative to decompression and adiabatic rapid passage for future microgravity experiments. We are currently exploring the viability of directly producing a BEC in such a trap. A BEC in a three-dimensional quartic trap (as given near the minimum of the QZ potential and in the absence of gravity) is expected to have a substantially flatter condensate density profile near the centre as compared to that of a harmonically trapped condensate[43], presenting opportunities to observe transitions and phases of quantum matter in a relatively homogeneous system. Also, we recognize that the absence of the first-order Zeeman shift for atoms in magnetically insensitive states makes these gases

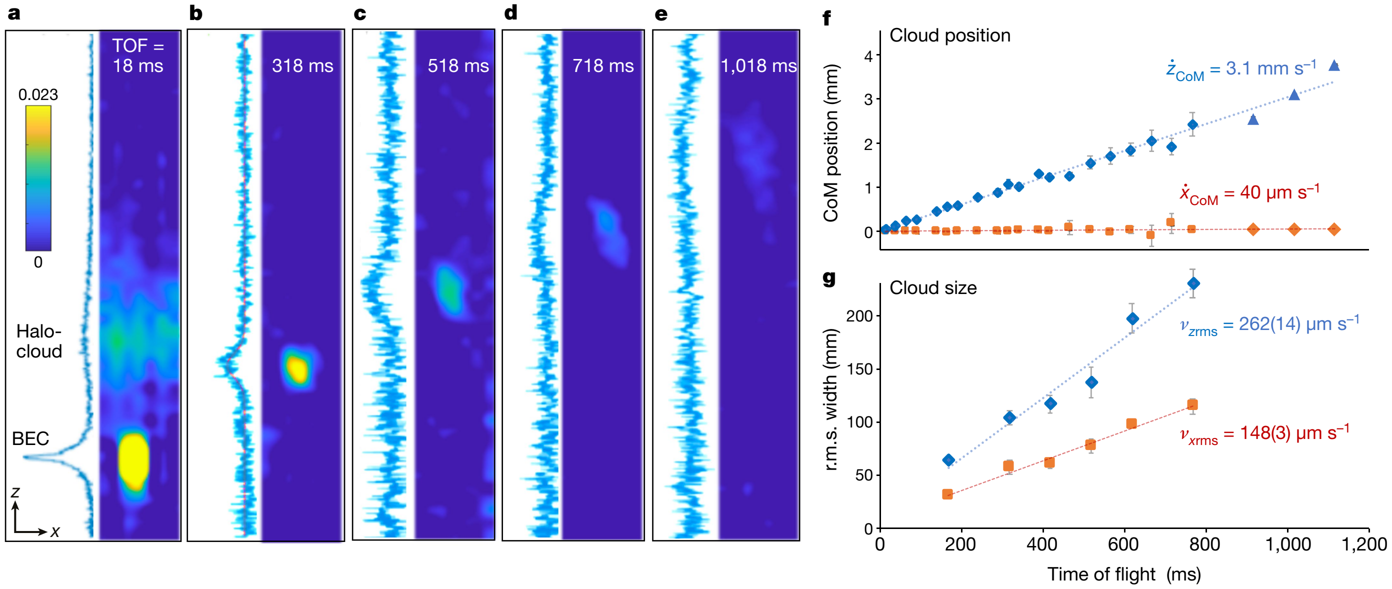

Fig. 4 | In-orbit free expansion of ultracold atoms. a–**e**, Each panel shows a density profile (left) and an absorption image of ^{87}Rb atoms (right) after increasing free expansion times (TOF in ms: **a**, 18; **b**, 318; **c**, 518; **d**, 718; **e**, 1,018) in persistent microgravity. In **a**, a bimodal distribution of condensed atoms (a BEC) is seen in the absorption image, and a residual cloud of $|2, 0\rangle$ atoms ('halo-cloud') is drifting up and away from the BEC at more than 50 mm s^{-1}. A post-processing method of array reduction through bicubic interpolation increases the contrast of the atom signal to reveal atoms with TOF > 1 s (see Methods). The density scale is constant across these absorption images, selected so that the atom signal is still distinguishable from the image background for the atom clouds that have undergone the longest free expansion time. An adjusted density scale for each expansion time is shown to the left of each image, plotting the horizontal sums of the pixels with no applied interpolation. **f**, Plot of centre-of-mass (CoM) position ('Cloud position') versus time of flight yields the residual centre-of-mass velocities, $\dot{x}_{\mathrm{CoM}} = 40$ µm s^{-1} (red) and $\dot{z}_{\mathrm{CoM}} = 3.1$ mm s^{-1} (blue). **g**, Plot of r.m.s. width ('Cloud size') versus time of flight shows the residual expansion of the BEC, corresponding to kinetic energies of 231(9) pK and 720(79) pK (along x and z, respectively), derived from the cloud expansion rates, $v_{x\mathrm{rms}} = 148(3)$ µm s^{-1} and $v_{z\mathrm{rms}} = 262(14)$ µm s^{-1}, measured between 168 ms to 768 ms TOF. Error bars, ±1 s.d. with $n \geq 3$ (see Methods).

highly immune to frequency shifts and broadening of spectral lines from stray magnetic fields and gradients respectively, and so uniquely suited for high-precision spectroscopy and applications requiring long atomic-state coherence times[44,45]. The prospect of confining and manipulating atoms already prepared in magnetically insensitive states without the need for an optical trap therefore presents a more subtle but still enabling advantage of microgravity for next-generation precision metrology with quantum gases.

We have used the baseline capabilities of CAL in low Earth orbit to demonstrate immediate and fundamental benefits of microgravity for ultracold atom experiments, including demonstration of novel evaporation regimes and by-products, free-space BEC expansion times over one second in duration, and decompression-cooled condensates with picokelvin effective temperatures. These experiments form the start of potentially years of science operations, with additional capabilities of the instrument to be employed over time. The first series of experiments is currently underway, using ^{87}Rb to study bubble-shell geometries and investigate applications of atom interferometry for future precision measurements in the areas of Earth observation and fundamental physics[4–6,9–11]. The on-orbit production of ^{87}Rb BEC using RF evaporation reported here sets the stage for production of ^{87}Rb BECs via microwave evaporation, and the subsequent sympathetic cooling of potassium[40]. With this capability comes additional prospects for interferometry[9], the utilization of Feshbach resonances to control differential centre-of-mass distributions of dual-species quantum gas mixtures[8,12], and few-body systems in new temperature and density regimes that are prerequisites for the next generation of Efimov experiments[7,8]. Meanwhile, future modular upgrades for the CAL instrument are available for extended mission studies, including a science module built by JPL featuring an atom-wave interferometer. Additionally, payloads for follow-on missions are in proposal and development stages[46], assuring the continued presence and application of ultracold atoms in orbit.

Online content

Any methods, additional references, Nature Research reporting summaries, source data, extended data, supplementary information, acknowledgements, peer review information; details of author contributions and competing interests; and statements of data and code availability are available at https://doi.org/10.1038/s41586-020-2346-1.

1. Leanhardt, A. E. et al. Adiabatic and evaporative cooling of Bose–Einstein condensates below 500 picokelvin. *Science* **301**, 1513–1515 (2003).
2. Ammann, H. & Christensen, N. Delta kick cooling: a new method for cooling atoms. *Phys. Rev. Lett*. **78**, 2088–2091 (1997).
3. Safronova, M. et al. Search for new physics with atoms and molecules. *Rev. Mod. Phys*. **90**, 025008 (2018).
4. Lundblad, N. Microgravity dynamics of bubble-geometry Bose-Einstein condensates. *NASA Space Life and Physical Sciences Research and Applications Division Task Book* (2017); https://taskbook.nasaprs.com/tbp/tbpdf.cfm?id=11095.
5. Lundblad, N. et al. Shell potentials for microgravity Bose-Einstein condensates. *npj Microgravity* **5**, 30 (2019).
6. Meister, M., Roura, A., Rasel, E. M. & Schleich, W. P. The space atom laser: an isotropic source for ultra-cold atoms in microgravity. *New J. Phys*. **21**, 013039 (2019).
7. Cornell, E. Zero-g studies of few-body and many-body physics. *NASA Space Life and Physical Sciences Research and Applications Division Task Book* (2017); https://taskbook.nasaprs.com/tbp/tbpdf.cfm?id=11096.
8. D'Incao, J. P., Krutzik, M., Elliott, E. & Williams, J. R. Enhanced association and dissociation of heteronuclear Feshbach molecules in a microgravity environment. *Phys. Rev. A* **95**, 012701 (2017).
9. Bigelow, N. Consortium for ultracold atoms in space. *NASA Space Life and Physical Sciences Research and Applications Division Task Book* (2015); https://taskbook.nasaprs.com/tbp/tbpdf.cfm?id=10085.
10. Sackett, C. Development of atom interferometry experiments for the International Space Station's cold atom laboratory. *NASA Space Life and Physical Sciences Research and Applications Division Task Book* (2017); https://taskbook.nasaprs.com/tbp/tbpdf.cfm?id=11097.
11. Sackett, C. A., Lam, T. C., Stickney, J. C. & Burke, J. H. Extreme adiabatic expansion in micro-gravity: modeling for the Cold Atomic Laboratory. *Microgravity Sci. Technol*. **30**, 155–163 (2018).
12. Williams, J. Fundamental interactions for atom interferometry with ultracold quantum gases in a microgravity environment. *NASA Space Life and Physical Sciences Research and Applications Division Task Book* (2017); https://taskbook.nasaprs.com/tbp/tbpdf.cfm?id=11101.
13. National Research Council in *Recapturing a Future for Space Exploration* 249–262 (National Academies Press, 2011).
14. Kovachy, T. et al. Matter wave lensing to picokelvin temperatures. *Phys. Rev. Lett*. **114**, 143004 (2015).
15. Kovachy, T. et al. Quantum superposition at the half-metre scale. *Nature* **528**, 530–533 (2015).
16. Müntinga, H. et al. Interferometry with Bose–Einstein condensates in microgravity. *Phys. Rev. Lett*. **110**, 093602 (2013).
17. van Zoest, T. et al. Bose–Einstein condensation in microgravity. *Science* **328**, 1540–1543 (2010).
18. Kulas, S. et al. Miniaturized lab system for future cold atom experiments in microgravity. *Microgravity Sci. Technol*. **29**, 37–48 (2017).
19. Condon, G. et al. All-optical Bose–Einstein condensates in microgravity. *Phys. Rev. Lett*. **123**, 240402 (2019).
20. Stern, G. et al. Light-pulse atom interferometry in microgravity. *Eur. Phys. J. D* **53**, 353–357 (2009).
21. Barrett, B. et al. Dual matter-wave inertial sensors in weightlessness. *Nat. Commun*. **7**, 13786 (2016).
22. Altenbuchner, L. et al. MORABA—overview on DLR's mobile rocket base and projects. In *Proc. SpaceOps 2012 Conf*. (American Institute of Aeronautics and Astronautics, 2012); https://doi.org/10.2514/6.2012-1272497.
23. Schkolnik, V. et al. A compact and robust diode laser system for atom interferometry on a sounding rocket. *Appl. Phys. B* **122**, 217 (2016).
24. Lezius, M. et al. Space-borne frequency comb metrology. *Optica* **3**, 1381–1387 (2016).
25. Dinkelaker, A. N. et al. Autonomous frequency stabilization of two extended-cavity diode lasers at the potassium wavelength on a sounding rocket. *Appl. Opt*. **56**, 1388–1396 (2017).
26. Becker, D. et al. Space-borne Bose–Einstein condensation for precision interferometry. *Nature* **562**, 391–395 (2018).
27. Williams, J. R., Chiow, S.-W., Yu, N. & Müller, H. Quantum test of the equivalence principle and space-time aboard the international space station. *New J. Phys*. **18**, 025018 (2016).
28. Aguilera, D. N. et al. STE-QUEST-test of the universality of free fall using cold atom interferometry. *Class. Quantum Gravity* **31**, 115010 (2014).
29. Kolkowitz, S. et al. Gravitational wave detection with optical lattice atomic clocks. *Phys. Rev. D* **94**, 124043 (2016).
30. Hogan, J. M. & Kasevich, M. A. Atom-interferometric gravitational-wave detection using heterodyne laser links. *Phys. Rev. A* **94**, 033632 (2016).
31. Hogan, J. M. et al. An atomic gravitational wave interferometric sensor in low Earth orbit (AGIS-LEO). *Gen. Relativ. Gravit*. **43**, 1953–2009 (2011).
32. Yu, N. & Tinto, M. Gravitational wave detection with single-laser atom interferometers. *Gen. Relativ. Gravit*. **43**, 1943–1952 (2011).
33. Kómár, P. et al. A quantum network of clocks. *Nat. Phys*. **10**, 582–587 (2014).
34. Elder, B. et al. Chameleon dark energy and atom interferometry. *Phys. Rev. D* **94**, 044051 (2016).
35. Yu, N., Kohel, J. M., Kellogg, J. R. & Maleki, L. Development of an atom-interferometer gravity gradiometer for gravity measurement from space. *Appl. Phys. B* **84**, 647–652 (2006).
36. Sorrentino, F. et al. The space atom interferometer project: status and prospects. *J. Phys. Conf. Ser*. **327**, 012050 (2011).
37. Chiow, S.-W. & Yu, N. Compact atom interferometer using single laser. *Appl. Phys. B* **124**, 96 (2018).
38. Battelier, B. et al. Development of compact cold-atom sensors for inertial navigation. *Proc. SPIE Quant. Opt*. **9900**, 990004 (2016).
39. Fang, B. et al. Metrology with atom interferometry: inertial sensors from laboratory to field applications. *J. Phys. Conf. Ser*. **723**, 012049 (2016).
40. Elliott, E. R., Krutzik, M. C., Williams, J. R., Thompson, R. J. & Aveline, D. C. NASA's Cold Atom Lab (CAL): system development and ground test status. *npj Microgravity* **4**, 16 (2018).
41. Farkas, D. M., Salim, E. A. & Ramirez-Serrano, J. Production of rubidium Bose–Einstein condensates at a 1 Hz rate. Preprint at http://arXiv.org/abs/1403.4641v2 (2014).
42. Jenkins, F. A. & Segrè, E. The quadratic Zeeman effect. *Phys. Rev*. **55**, 52–58 (1939).
43. Chaudhary, G. K., Chattopadhyay, A. & Ramakumar, R. Bose–Einstein condensate in a quartic potential: static and dynamic properties. Int. *J. Mod. Phys. B* **25**, 3927–3940 (2012).
44. Tino, G. & Kasevich, M. *Atom Interferometry* (IOS Press, 2014).
45. Côté, R., Gould, P. L., Rozman, M. & Smith, W. S. (eds) Precision measurements. In *Pushing the Frontiers of Atomic Physics: Proc. XXI Int. Conf. on Atomic Physics*, 47–87 (World Scientific, 2009).
46. Frye, K. et al. The Bose–Einstein condensate and cold atom laboratory. Preprint at http://arXiv.org/abs/1912.04849 (2019).

Publisher's note Springer Nature remains neutral with regard to jurisdictional claims in published maps and institutional affiliations.

© The Author(s), under exclusive licence to Springer Nature Limited 2020

Methods

CAL utilizes two imaging systems that collect data on the atom density for rubidium and potassium. While mainly used for absorption imaging, they are also able to collect fluorescence images in order to assess the magneto-optical trap (MOT) status and monitor laser powers. The primary system images along the surface of the chip (*y* axis) by applying two pulses of laser light separated by nominally 54 ms with a pulse duration of 40 µs. Circularly polarized imaging light, 'Imaging (*y*)' in Fig. 1, is directed along the *y* axis together with an applied magnetic field. All the data presented in this Article were collected by this primary system. An orthogonal angle of view is available, labelled 'Imaging (*z*)' in Fig. 1, and is collected through the atom chip window. For the purpose of displaying images of the atom signal at long expansion times (as in Fig. 4), contrast between the atom cloud and the image background is increased by reducing the number of pixels in the image using bicubic interpolation and anti-aliasing. Specific details of this process can be found in the kernel for MATLAB's 'imresize' function. The data taken at free expansion times of 918 ms, 1,018 ms and 1,118 ms are first processed with these methods, and then the centre of mass extracted (depicted as triangles in Fig. 4f). The rest of the data's error bars represent standard deviations from multiple shots with $n \geq 3$. Widths of the atomic cloud, which are used to determine momentum, are found from two-dimensional Gaussian fits to images that undergo no resizing (data with free expansion times of 168 ms to 768 ms).

The dual-cell vacuum chamber is based on ColdQuanta's commercially offered RuBECi[41], which is augmented for CAL-specific science objectives and space flight compatibility. The source cell contains rubidium and potassium alkali metal dispensers with natural abundance of the isotopes. The MOT is formed in the UHV science cell approximately 15 mm below the chip surface using three incident beams that are retro-reflected to create a six-beam three-dimensional MOT. Extended Data Fig. 1a illustrates the MOT location in the science cell, and the four optical beams that are incident upon atoms in the *y*–*z* plane. More details about the hardware and configuration can be found in the referenced material[40,41]. From the MOT, the atoms are gathered in a quadrupole magnetic trap formed by external coils and then transported along the *z* axis to the atom chip.

The first-order magnetic potential for ^{87}Rb atoms in the $F = 2$ hyperfine manifold is proportional to the product of the field modulus and the magnetic quantum number of the atom, m_F. Depending on the sign of m_F, the corresponding Zeeman state will be confined towards (+) or repelled from (−) a field minimum in the chip-trap. An applied RF field (the RF knife) then couples the trapped atoms in the $|F = 2, m_F = 2\rangle$ state to the less confined $|2, 1\rangle$, the magnetically insensitive $|2, 0\rangle$, or the anti-trapped $|2, -1\rangle$ and $|2, -2\rangle$ states.

During CAL's evaporation stages, the magnetic trap is formed by applying bias fields along the *x* and *y* axes (Fig. 1f) that combine with the atom chip fields to yield relatively large trap oscillation frequencies for ^{87}Rb atoms in the $|2, 2\rangle$ state, which, near the approximately harmonic trap bottom of 7 G, correspond to trap oscillation frequencies $(\omega_x, \omega_y, \omega_z) = 2\pi \times (216, 1{,}000, 1{,}080)$ Hz. With such tight traps, collisions among atoms are sufficiently high to cool atoms to BEC in just over a second of evaporation time. For the $|2, 0\rangle$ state, these same fields form an attractive QZ potential for the $|2, 0\rangle$ state with an 18 µK depth. Similar to the $|2, 2\rangle$ trap, with a trap aspect ratio of $\sqrt{\langle x_z^2\rangle/\langle x_x^2\rangle} = \sqrt{\omega_x^2/\omega_z^2} = 0.2$, any $|2, 0\rangle$ atoms confined by the QZ force and able to exchange energy between dimensions should produce an aspect ratio of ≤0.2, which is lower than that of the original harmonic trap due to the additional quartic terms.

Following forced evaporation we apply two stages of decompression in orbit, during which we apply a linear decrease to the magnetic bias fields down to 12% of their evaporation values over the first 100 ms, then further decrease the bias fields to 8% with a second stage, varied from 100 ms to 200 ms in duration. These two decompression stages lower the trap oscillation frequencies for the $|2, 2\rangle$ state to $(\omega_x, \omega_y, \omega_z) = 2\pi \times (8.2, 30, 46)$ Hz and $(\omega_x, \omega_y, \omega_z) = 2\pi \times (11, 20, 15)$ Hz, respectively. Chip currents are held constant during all decompression protocols reported in the current work, and then all chip currents are extinguished within 20 µs in order to release atoms for free expansion and imaging after varied time of flight. The second decompression ramp time of 181 ms was empirically determined to limit centre-of-mass motion to a drift velocity of 3.1 mm s^{-1}. We then perform 3 ms of adiabatic rapid passage into the $|2, 0\rangle$ state to minimize forces from stray magnetic gradients.

Stringent requirements on the design and implementation of CAL were required to not only satisfy the size, weight, power and thermal management requirements of the ISS, but also to assure robust and reproducible operation over its lifetime in the variable ISS environment. CAL incorporates relatively high repetition rates with long-term operation (running hundreds of times each day for over 1.5 years). These features provide large and repeatable datasets with iterative feedback capabilities necessary for advancing the scientific and technical maturation of microgravity-enabled atomic gas experiments. The total volume (0.4 m^3) and mass (233 kg) were optimized to allow CAL to occupy one single locker and one quad-locker of an EXPRESS rack (as illustrated in Fig. 1). The average daily power draw for all CAL subsystems is 510 W. For thermal management of the laser and electronics subsystems, as well as for the vacuum chamber inside the science module, air and water cooling are used at supply temperatures of 18 °C.

In contrast to analogous terrestrial and microgravity cold-atom systems demonstrated to date, CAL is designed to operate for years in a highly dynamic environment without regular human intervention. Access to this orbital environment, relatively high duty cycles, and mitigation of external perturbations allows investigators to pursue longer microgravity-enabled experimental campaigns and demonstrates advances in technology towards exploring fundamental science that is inaccessible on the ground (including geodesy with atomic test masses and high-precision tests of the underlying principles of Einstein's general relativity). Magnetic shielding inside the science module is designed to mitigate the effects of the Earth's magnetic field, which varies in both direction and amplitude over each 90-min orbit. In parallel, the excessive radiation environment (for example, during passes through the South Atlantic Anomaly), local perturbations from neighbouring experiments on the ISS and from astronaut activities, the high rotation rate of the ISS, and the intense vibration and acoustic environments during launch were all accounted for in the design of CAL.

Data availability

Source data for Fig. 4 are provided with the paper. The datasets generated and analysed during the current study are available from the corresponding authors on reasonable request.

Acknowledgements We gratefully acknowledge the contributions of current and former members of CAL's management and technical teams, T. Winn, K. Muse, L. Clonts, J. Lam, J. Liu, C. Tran, J. Tarsala, T. Tran, S. Haque, M. McKee, J. Trager, J. Mota, G. Miles, D. Strekalov, I. Li, S. Javidnia, A. Sengupta, D. Conroy, A. Croonquist, E. Burt, M. Krutzik, S. Kulas and V. Schkolnik, and the ColdQuanta team, including E. Salim, L. Czaia, J. Ramirez-Serrano, J. Duggan, and D. Anderson. We recognize the continuing support of JPL's Astronomy, Physics and Space Technology Directorate, L. Livesay, T. Gaier, D. Coulter, C. Lawrence and U. Israelsson. We thank CAL's principal investigators and science team members, N. Bigelow, N. Lundblad, C. Sackett, E. Cornell, P. Engels and M. Mossman, for their guidance, along with CAL's Science Review Board, including B. DeMarco and R. Walsworth. We also recognize the steadfast support from NASA's Division of Space, Life, and Physical Sciences Research and Applications (SLPSRA), C. Kundrot, D. Malarik, M. Lee, B. Carpenter and D. Griffin. This work was funded by NASA's SLPSRA programme office, and operated by the Jet Propulsion Laboratory, California Institute of Technology, under contract with NASA. US Government sponsorship is acknowledged.

Author contributions D.C.A., J.R.W. and E.R.E. optimized and operated the instrument during the CAL commissioning phase, collected and analysed the associated data, and prepared this manuscript. D.C.A., J.R.W. and E.R.E. were responsible for instrument hardware integration, experimental operation, optimization and data acquisition during the CAL integration and test phase. D.C.A. led CAL's ground testbed and the integration and testing of the science module

hardware. J.R.W. led flight instrument operation and atom-interferometer-related tests. E.R.E. led integration and operation of CAL's engineering model testbed. C.D. established and led the mission operations and ground data systems during commissioning. J.R.K. prepared and coordinated ISS installation procedures and operations. J.R.K. and J.M.K. led the laser and optics subsystems and operated the system post-commissioning. R.F.S., K.O., N.Y. and N.E.L. led technical planning and provided guidance across multiple subsystems during the integration and test phase. R.J.T. proposed the instrument, gave scientific guidance and coordinated with principal investigators as CAL project scientist. All authors read, edited and approved the final manuscript.

Competing interests The authors declare no competing interests.

Additional information

Correspondence and requests for materials should be addressed to D.C.A. or R.J.T.

Peer review information *Nature* thanks A. Roura and the other, anonymous, reviewer(s) for their contribution to the peer review of this work.

Reprints and permissions information is available at http://www.nature.com/reprints.

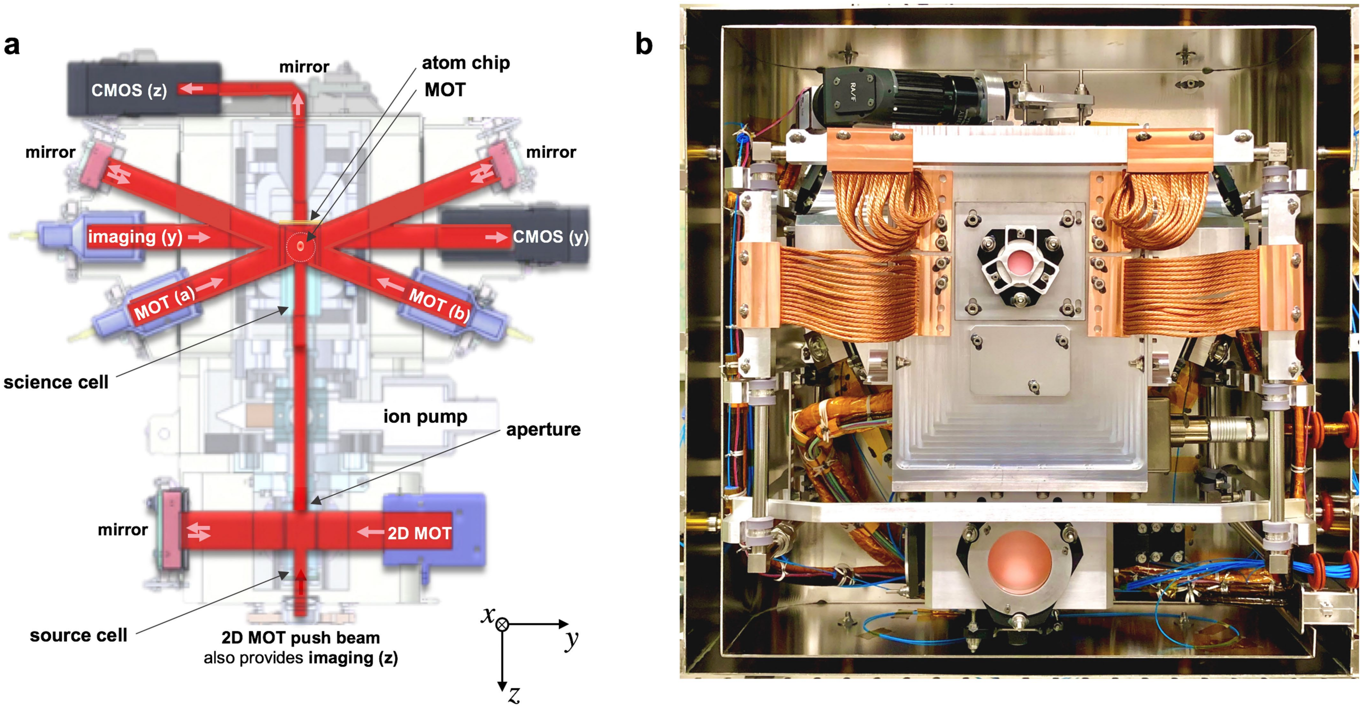

Extended Data Fig. 1 | Science module optical beams. **a**, An illustrative cross-section of the science module in the y–z plane, showing the optical beam paths for laser cooling and imaging. Collimators (depicted in blue) each accept optical fibre inputs and direct free-space beams into the vacuum chamber. In the source cell, elliptical beam collimators create a two-dimensional (2D) MOT (the x-axis collimator is not shown). A cold atomic beam is directed (its flux enhanced by the 2D MOT push beam) up to the UHV science cell, where $>10^9$ atoms are collected in a three-dimensional MOT. In this region, laser cooling beams labelled 'MOT (a)' and 'MOT (b)' are directed along the y–z plane, while a third collimator (not shown) sends its 11-mm-diameter beam (dotted circle) along the x-axis to complete the MOT. Each beam is retro-reflected by a mirror to create a full six-beam MOT located about 15 mm below the atom chip, which forms the topmost wall of the UHV chamber. CAL's primary imaging beam (also 11 mm in diameter) is directed parallel to the chip surface along the y axis just under the chip, labelled as 'Imaging (y)'. Fluorescence and absorption images along this axis are collected on the 'CMOS (y)' camera. Alternatively, through-chip imaging along the z axis can be collected by the 'CMOS (z)' camera, with an absorption imaging beam provided by the 'Imaging (z)' light that passes through a 0.75-mm-diameter aperture of the source cell. This aperture provides differential pumping to maintain UHV conditions in the science cell while the source cell runs at higher pressures of Rb and K. The background pressure of Rb and K is controlled by running independent current through each of two alkali metal dispensers: one containing Rb, and the other K. Atoms are collected in the MOT before undergoing molasses cooling and becoming confined by the coil-generated magnetic trap. The trapped cloud is then transported up 15 mm by a second pair of coils, and then loaded into the atom chip trap. **b**, A photograph of a science module without its front clam-shell of magnetic shields, showing the mechanical structure that rigidly supports the vacuum and optical hardware, as well as some of the thermal management components. More details of the science module and control hardware can be found in ref. [40].